Mechanistic Study of Chemical Deposition of ZnS Thin Films from Aqueous Solutions Containing Zinc Acetate and Thioacetamide by Comparison with Homogeneous Precipitation

Koichi Yamaguchi,[†] Tsukasa Yoshida,*[,†] Daniel Lincot,[‡] and Hideki Minoura[†]

Environmental and Renewable Energy Systems (ERES) Division, Graduate School of Engineering, Gifu University, Yanagido 1-1, Gifu 501-1193, Japan, and Laboratoire d'Electrochimie et de Chimie Analytique (UMR 7575), Ecole Nationale Supérieure de Chimie de Paris, 11 rue Pierre et Marie Curie, 75231 Paris Cedex 05, France

Received: February 22, 2002; In Final Form: October 21, 2002

Chemical bath deposition of ZnS thin films (CBD) in zinc acetate-thioacetamide (TAA) aqueous solutions has been studied in the temperature range between 50 and 90 °C. The rate of film growth is compared to that of homogeneous precipitation of ZnS. The film growth was found to proceed by accumulation of ZnS nanocrystallites (4 nm) formed in the solution according to a cluster-by-cluster mechanism. The rate of the precipitation reaction in the present system has been phenomenologically well described by the rate equation, $dP_t/dt = k[Zn(II)]^n[TAA]^n$, where P_t is the concentration of ZnS precipitate at time t, k is the temperature-activated reaction rate constant, and n is the apparent reaction order, which was determined as 0.64. The same rate equation was successfully applied to the film growth based on the assumption that the rate of the film growth is proportional to that of the precipitation, i.e., $F_t = mP_t$, where F_t is the film thickness at time t and m is a proportionality factor. This result shows that the rate of the film growth is under the control of ZnS precipitation in the solution. However, linear increase of m has been found when the ratio of initial concentrations of the two components, $[Zn(II)]_0/[TAA]_0$, is larger than unity, indicating the increase in the rate of the film growth, while m remains constant when $[Zn(II)]_0/[TAA]_0$ is less than unity. The variation of m and the coincident morphological change of both the film and the precipitate indicate enhanced aggregation of ZnS nanocrystallites in the presence of excess zinc ion, which is most likely explained by a decrease of the repulsive electrostatic force among ZnS nanocrystallites by charge neutralization. The rate-limiting step for the formation of ZnS clusters is attributed to the initial decomposition of a complex between zinc acetate and thioacetamide species.

Introduction

Fabrication of thin films from solutions, i.e., under atmospheric pressure and at near room temperature, is beneficial for both economical and ecological reasons, compared to conventional vapor phase techniques which require much energy.[1] Chemical[2−26] and electrochemical[23−33] deposition of compound semiconductor thin films from solutions has been actively studied, especially for chalcogenide materials. Primary applications presently concern their use for the preparation of thin-film solar cells, where large area deposition processes at low costs are needed. As leading examples, one can mention the use of electrodeposition for the production of cadmium telluride layers[31−33] and the use of chemical bath deposition (CBD) for the production of CdS window layers[2,32] for both CdTe and $Cu(In,Ga)Se_2$ (called CIGS) cells. Zinc sulfide (ZnS) is presently emerging as potential candidate for replacing CdS layers in these photovoltaic cells.[14,15] Use of ZnS as a window layer allows a more effective photocurrent generation due to the larger band gap of ZnS (∼3.6 eV) than that of CdS (∼2.4 eV) and benefits also for the fabrication of cadmium-free CIGS devices. ZnS is also an important II−VI compound semiconductor, finding applications in other fields as deep-blue light emitting devices[34] or a base material for phosphors.[35,36] The key point of the recent success of ZnS in thin-film solar cells is the use of a CBD technique for the film deposition, as a high conversion efficiency was achieved with the CdS thin films prepared by CBD. However, in contrast to the case of CdS, studies on the film growth for ZnS are more limited, and the level of understanding of the deposition mechanism is much lower. The aim of this paper is to bring a contribution in this field, based on a systematic parametric study, from which some specific aspects of the growth processes can be extracted and discussed.

The preparation of ZnS films by chemical bath deposition started to develop about a decade ago.[2] The films are generally prepared by using the reaction between zinc ions and thiourea (TU) or thioacetamide (TAA) in hot basic solutions. In the Zn^{2+}−thiourea−NH_3 system, for instance, the overall reaction can be expressed as eq 1.

$$Zn(NH_3)_n^{2+} + SC(NH_2)_2 + 2\,OH^- \rightarrow ZnS + NH_2CN + 2H_2O + nNH_3 \quad (1)$$

Two distinct models have been proposed for the growth mechanism in CBD.[2,11,12] In the case of CdS, this reaction was demonstrated to proceed via surface sites involving directly the precursor species (atom-by-atom growth or heterogeneous

* Corresponding author. Fax +81-(0)58-293-2587; e-mail yoshida@apchem.gifu-u.ac.jp.
[†] Gifu University.
[‡] Ecole Nationale Supérieure de Chimie de Paris.

10.1021/jp025676q CCC: $25.00
Published on Web 12/03/2002

precipitation by analogy with precipitation concepts). In the case of ZnS, the growth of the film is mostly considered as the result of surface aggregation of colloids formed in the solution (cluster-by-cluster growth). This constitutes the main difference between the two systems, which deserves further investigation.

As previous studies on CBD of ZnS were mostly focused on the film growth by itself,[11−23] our approach in this paper is to consider also the homogeneous precipitation phenomenon in detail, which takes place parallel to the film growth, and the relations between both aspects. Contrary to the film growth, the domain of ZnS precipitation from aqueous solutions has been extensively studied, and is still a very dynamic field of investigation.[35−45] In the 1980s, several groups studied the formation of monodispersed colloidal particles of ZnS, though internal structure of colloidal particles was not clarified. Later, Celikkaya and Akinc studied the formation of ZnS particles in an acidic aqueous mixture of Zn^{2+} and TAA.[40,41] Vacassy et al. obtained spherical particles of ZnS with a diameter of 1.5 μm by using solutions containing zinc dimethyldithiocarbamate and TAA.[36] In both studies, morphological and crystallographic analyses of ZnS particles have revealed that spherical particles of ZnS with diameters of a few μm are not single crystals but are made up of nanocrystallites that are formed in the solution phase.[36,41] Both groups have suggested that the growth of ZnS particles proceeds by the formation of nanocrystallites in the solution phase, followed by aggregation of these nanocrystallites. A recent model proposed by Eshuis et al. brings new insights in mechanistic aspects for the formation of colloidal ZnS particles.[43] The idea in this model is also applied for understanding the growth mechanism on the chemical bath deposition of indium hydroxide sulfide thin films, although the comparison of the resultant films to the precipitate formed in the bath has not been made.[7]

In our previous studies, it has been found that CBD of ZnS is possible in neutral baths or even in acidic baths containing Zn^{2+} salt and TAA,[20,23] which are indeed similar systems employed for the preparation of colloids. The overall reaction is expressed as eq 2, considering that acetonitrile is formed as a byproduct.[46,47]

$$Zn^{2+} + CH_3CSNH_2 = ZnS + CH_3CN + 2H^+ \qquad (2)$$

In this work, we have carried out a systematic analysis on both the film growth and the homogeneous precipitation in these conditions, using zinc acetate and thioacetamide (TAA) as precursors, where the pH of the reaction bath is neutral. The film growth in the present system proceeds in a typical cluster-by-cluster manner. The rate-limiting step is attributed to the initial reaction step, involving the decomposition of a 1:1 complex between a zinc ion and a TAA molecule, proceeding continuously in the bulk of the solution. The present study has revealed that the rate of the film growth is clearly related to the rate of formation of nanocrystallites in the homogeneous precipitation process as well as that of the aggregation process of the nanocrystallites at the surface.

Experimental Section

Materials. Doubly distilled and ion-exchanged pure water was used throughout the experiments. Zinc acetate, $Zn(CH_3COO)_2 \cdot 2H_2O$ ($Zn(OAc)_2$) of analytical reagent grade was purchased from Kishida Chemical Co., Ltd. and used as received. Thioacetamide (TAA) was purchased from Tokyo Chemical Industry Co., Ltd., recrystallized in benzene, and dried in vacuum before use.[38,47] Indium tin oxide (ITO) coated glass (10 Ω/sq, Musashino Fine Glass) was mainly used as the substrate. Glass substrates were also used for some experiments. The substrates were ultrasonically cleaned subsequently in acetone, 2-propanol, and water before the film deposition.

Deposition of ZnS. Aqueous solutions of both $Zn(OAc)_2$ and TAA were separately freshly prepared before each experiment. These two solutions were mixed in a glass reaction vessel and used as a bath for the film deposition. The final volume of the reaction bath was 30 mL. While the concentration of one (either $Zn(OAc)_2$ or TAA) was fixed to 0.1 M (M = mol/L), that of the other was varied as 0.025, 0.1, 0.2, and 0.4 M in the final mixture. Although no pH adjustment of the reaction bath was made, pH was about 6.5 for all solutions. A substrate (1.5 cm in width and 5.0 cm in length) was immersed vertically in the middle of the bath, and the reaction vessel was placed in a thermostat bath set at the desired temperature (between 50 and 90 °C). The deposition was carried out for controlled time periods up to 120 min. The reaction bath was not stirred during the film deposition. The deposited films were ultrasonically washed in water for 1 min, dried in air at room temperature, and subjected to further analyses.

Homogeneous Precipitation of ZnS. The chemical composition of the reaction baths used for the preparation of ZnS precipitate was the same as those used for the film deposition, while the experiments were performed in a larger volume (200 mL) without immersion of substrates. The ZnS precipitate that formed in the bath was filtered by a hydrophilic PTFE membrane filter (Advantec, pore size = 0.1 μm) and thoroughly washed by water. The precipitate was dried for 2 days in a desiccator containing silica gel at room temperature. The amount of ZnS precipitate was then measured by weighing the dried samples. For convenience, the amount of precipitate is expressed in mM (= 10^{-3} mol/L) in this paper by dividing the collected mass by the volume of the solution. Although particles smaller than 0.1 μm would go through the pore of the filter, we assume that the mass of those particles is negligible since the appearance of a bluish tint, probably due to the Rayleigh scattering, was observed during the reaction, which indicates that the diameter of the particle reaches about 0.1 μm as reported in the literature.[43] For example, in the case of a 0.1 M $Zn(OAc)_2$ + 0.1 M TAA at 70 °C, this phenomenon took place in only about 1 min.

Characterization of ZnS Films and Precipiates. X-ray diffraction (XRD) patterns were measured on a Rigaku Rad-2R X-ray diffractometer using Cu Kα radiation. The morphology of the films and precipitate was observed by using a TOPCON ABT-150FS scanning electron microscope (SEM). The fine structure and the electron diffraction pattern of the samples were observed by a Hitachi H-8100 transmission electron microscope (TEM). Absorption spectra were measured by a Hitachi U-3500 spectrophotometer. The film thickness was measured by a Kosaka Lab. Ltd. SE−2300 surface profilometer. The composition of ZnS films was analyzed by a Horiba EMAX-2770 energy-dispersive X-ray analyzer (EDX). Films with thicknesses of ca. 500 nm were obtained by repeating the deposition process using a freshly prepared bath for the composition analysis in order to suppress signals generated from the substrate. Commercial ZnS powder (Furuuchi Chemicals, purity 5N) was used as a standard material.

Results

(a) Homogeneous Precipitation. *Effect of Temperature*. Figure 1 shows the change of the amount of the precipitate with reaction time in 0.1 M $Zn(OAc)_2$ + 0.1 M TAA at the

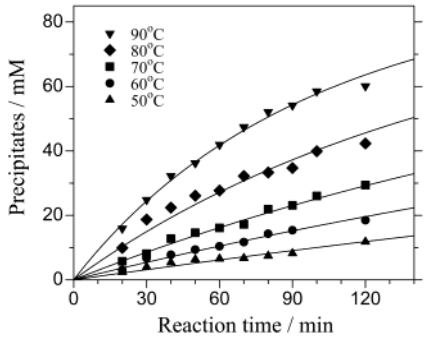

Figure 1. (a) Amounts of ZnS precipitate (P_t) plotted versus reaction time for reaction bath with $[Zn(II)]_0 = 0.1$ M and $[TAA]_0 = 0.1$ M at various bath temperatures of 50 °C (▲), 60 °C (●), 70 °C (■), 80 °C (♦), and 90 °C (▼). The solid lines are the fitting curves calculated by using eq 6 with $n = 0.637$ (see text for detail).

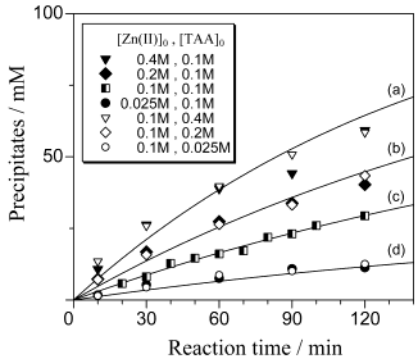

Figure 2. Amounts of ZnS precipitate (P_t) plotted versus reaction time for reaction baths with various compositions at 70 °C. One of $[Zn(II)]_0$ or $[TAA]_0$ was fixed to 0.1 M, while the other was varied as 0.025, 0.1, 0.2 and 0.4 M. Note the reversibility of $[Zn(II)]_0$ and $[TAA]_0$ to the rate of ZnS precipitation. The solid lines in the figure are the fitting curves according to the rate equation expressed by eq 5, for reversible combinations of $\{[Zn(II)]_0, [TAA]_0\}$: (a) {0.1M, 0.4 M}, (b) {0.1 M, 0.2 M}, (c) {0.1 M, 0.1 M}, and (d) {0.1 M, 0.025 M}. Optimum fitting to these experimental data has been obtained with $n = 0.637$ and a rate constant (k) of $5.66 \times 10{-3}$ $(\text{mol } l^{-1})^{1-2n}$ min^{-1} using eq 6 (see text for detail).

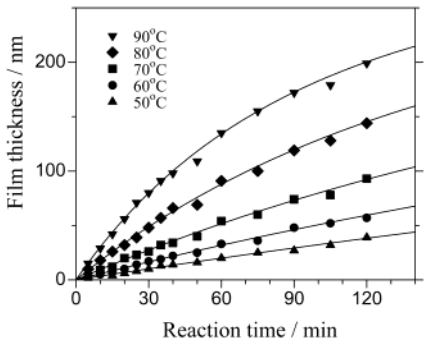

Figure 3. Thickness of ZnS thin films (F_t) plotted versus reaction time in reaction baths with $[Zn(II)]_0 = 0.1$ M and $[TAA]_0 = 0.1$ M. The depositions were carried out at various temperatures of 50 °C (▲), 60 °C (●), 70 °C (■), 80 °C (♦), and 90 °C (▼) (conditions equivalent to those of Figure 1). The solid lines indicate the fitting curves according to eq 7 which express that the film thickness is proportional to the amount of precipitate (see text). A temperature-independent proportionality factor m of 3.17 nm mM^{-1} has been determined as an optimum value for this bath composition.

temperature between 50 and 90 °C. The procedures to obtain the fitting curves in Figures 1-4 will be explained later in the phenomenological analysis section. There is a continuous increase of the amount of the precipitate with reaction time,

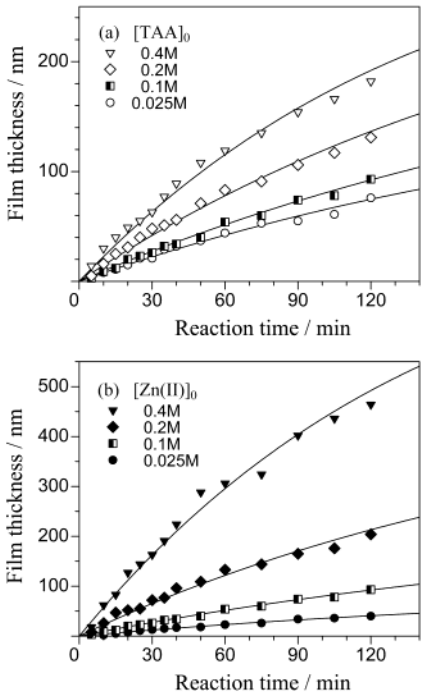

Figure 4. Thickness of ZnS thin films (F_t) plotted versus reaction time in the reaction baths for which $[Zn(II)]_0 = 0.1$ M while varying $[TAA]_0$ as 0.4, 0.2, 0.1, and 0.025 M (a), and $[TAA]_0 = 0.1$ M while varying $[Zn(II)]_0$ as 0.4, 0.2, 0.1 and 0.025 M (b). The film depositions were carried out at 70 °C. Note the differences of the rates of film growth in the reaction baths for which the concentrations of $Zn(OAc)_2$ and TAA are reversed, thus those having the same rate of ZnS precipitation (compare to Figure 3). Curve fittings were made according to eq 7 with variable m for optimum relationship between F_t and P_t for given bath compositions.

while the rate of precipitation gradually decreases. It is also clearly seen that the homogeneous precipitation rate is activated at the higher reaction temperature. One can note that after the reaction of 120 min at 90 °C, about 60% of the initial zinc content in solution is precipitated.

Effect of Bath Composition. Figure 2 shows the effect of $Zn(OAc)_2$ and TAA concentrations on the precipitation kinetics at 70 °C. In the first set of experiments (filled symbols) the initial concentration of TAA, $[TAA]_0$, was maintained constant at 0.1 M, whereas that of $Zn(OAc)_2$, $[Zn(II)]_0$, was varied between 0.025 and 0.4 M. We observe an increase of the precipitation rate as expected. In the second set of experiments (open symbols) the concentration variations are reversed between TAA and $Zn(OAc)_2$. We also observe an increase in the precipitation rate, but the most striking fact is that the change of the amount of the precipitate with time almost coincides in the two sets of experiments. This means that, from a kinetic point of view, the concentrations of $Zn(OAc)_2$ and TAA have the same effect.

(b) Film Growth. *Temperature Dependence*. Figure 3 shows variation of the rate of the film growth under conditions equivalent to those in Figure 1, i.e., in aqueous solutions of 0.1 M $Zn(OAc)_2$ + 0.1 M TAA maintained at the temperatures of 50, 60, 70, 80, and 90 °C. The change of the film thickness with reaction time at each temperature appears very similar to that of the amount of the precipitate (Figure 1), indicating similar thermal activation. The thickness of the film reaches about 200 nm after the reaction for 120 min at 90 °C.

Effect of Bath Composition. The rate of the film growth has also been studied in baths with various combinations of $[Zn(II)]_0$ and $[TAA]_0$, while maintaining the reaction temperature

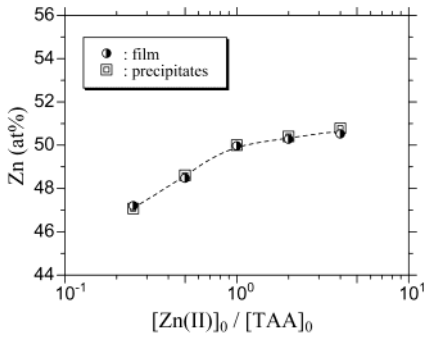

Figure 5. Chemical compositions of ZnS films and precipitate obtained in the baths with various $[Zn(II)]_0/[TAA]_0$ ratios.

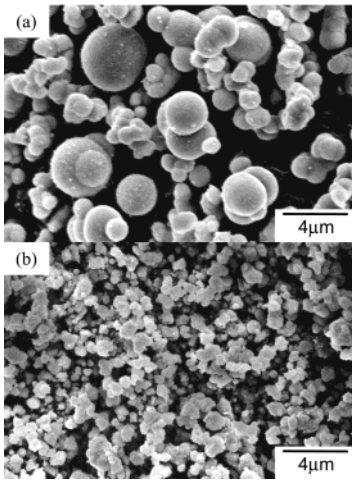

Figure 6. SEM images of ZnS precipitate formed in the baths for which $[Zn(II)]_0$ and $[TAA]_0$ were adjusted to 0.4 and 0.1 M (a), and 0.1 and 0.4 M (b), respectively. The reactions were carried out at 70 °C for 1 h. Note the difference of the particle size despite the same rate of precipitation under these two conditions.

constant (70 °C). Figures 4a and 4b show the plots of film thickness versus reaction time for the series varying $[TAA]_0$ while fixing $[Zn(II)]_0 = 0.1$ M and those varying $[Zn(II)]_0$ while fixing $[TAA]_0 = 0.1$ M, respectively. We observe that the growth rate increases with the precursor concentrations, as expected. As compared to the homogeneous process, it appears that the equivalence between the TAA and the $Zn(OAc)_2$ concentrations is not complete, especially in the highest concentration domain. For instance, the thickness of the films deposited under the two extreme deposition conditions, i.e., $[Zn(II)]_0/[TAA]_0 = 0.4$ M/0.1 M and $= 0.1$ M/0.4 M, reach 480 and 180 nm, respectively, after the reaction for 120 min.

(c) Characterization of ZnS Film and Precipitate. *Composition Analysis*. Chemical composition of ZnS thin film and precipitate under various bath compositions was analyzed by EDX (Figure 5). When the baths contain excess of TAA, the products tend to be slightly sulfur rich, probably due to the inclusion of unreacted TAA molecules. As $[Zn(II)]_0$ increases to achieve $[Zn(II)]_0/[TAA]_0 = 1$, the Zn content increases to achieve stoichiometric composition of ZnS (Zn/S = 50/50). Further increase of $[Zn(II)]_0$ only slightly increases the Zn content of the products, bearing almost stoichiometric compositions both for the film and the precipitate even at the highest $[Zn(II)]_0$.

Morphologies. Figures 6 and 7 present the morphologies of the precipitate and the films prepared under the two extreme conditions: $([Zn(II)]_0/[TAA]_0 = 0.4$ M/0.1 M and 0.1 M/0.4 M). The morphologies are very different in the two cases.

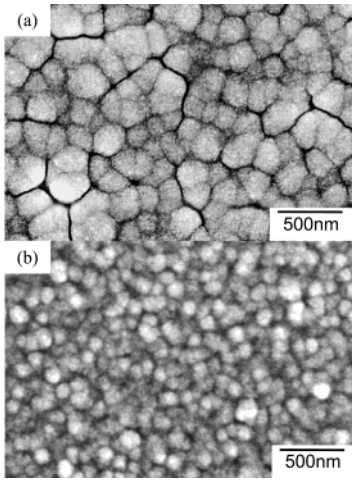

Figure 7. SEM images of ZnS thin films deposited under the same conditions as those in Figure 6, namely, $[Zn(II)]_0/[TAA]_0 = 0.4$ M/0.1 M (a), and 0.1 M/0.4 M (b) with the reaction time and temperature of 1 h and 70 °C, respectively. The difference in the size of the aggregates follows the trend seen for the precipitate in Figure 6.

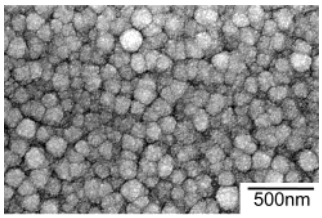

Figure 8. An SEM image of a ZnS thin film deposited in a bath with the standard composition, 0.1 M $Zn(OAc)_2$ + 0.1 M TAA, for 120 min at 70 °C.

Considering first the precipitate, it appears that the grain size increases markedly with the zinc content. The precipitate obtained in the bath with excess zinc ion consists of large spherical particles with diameters varying between 1 and 5 μm (Figure 6a). By contrast, much smaller particles with diameters of around 0.5 μm are produced with excess TAA ($[Zn(II)]_0/[TAA]_0 = 0.1$ M/0.4 M) (Figure 6b). It should be noted that the masses of the precipitate formed in these two solutions are almost the same in a given reaction time (Figure 2).

The film deposited with excess zinc is made of aggregates of around 250 nm in diameter (Figure 7a), whereas much finer aggregates of about 50 nm comprise the film deposited with excess TAA (Figure 7b). The morphology of the film appears to follow the same trend as that of the precipitate. As it is revealed later by the XRD analysis and TEM observation, both the precipitate and the film are made as aggregates of nanosized ZnS crystallites. The apparent smaller size of the aggregates in the film than that of the precipitate can be attributed to the geometrical restriction in the aggregation process in the case of the film growth. While the spherical shape of the precipitate indicates its isotropic growth, which reflects the three-dimensional diffusion of the ZnS nanocrystallites in solution, the shape of the aggregates in the film appears hemispherical as they are immobilized on a two-dimensional substrate. However, as the aggregates grow, they merge together to restrict their lateral growth so that the film growth eventually becomes unidirectional, being under control of the mass transport vertical to the substrate plane. Figure 8 shows the surface structure of a film deposited under the standard conditions ($[Zn(II)]_0/[TAA]_0 = 0.1$ M/0.1 M) on an ITO substrate for a film grown at 70 °C after reaction for 120 min. The fine morphology is close to that of low zinc conditions, with small grains agglomerated in larger

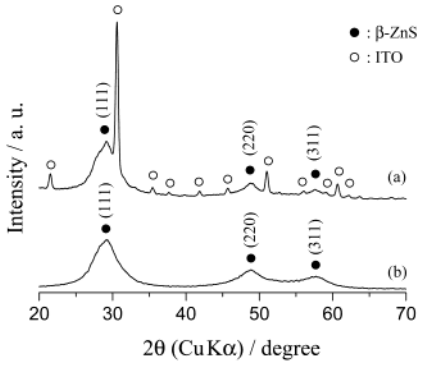

Figure 9. X-ray diffraction patterns of a ZnS thin film deposited on an ITO glass in a 0.1 M $Zn(OAc)_2$ + 0.1 M TAA aqueous mixture after a reaction for 240 min at 70 °C (a) and ZnS precipitate formed in the same reaction bath (b).

TABLE 1: Crystallite Size of ZnS Precipitates for Different Bath Composition and Reaction Temperature (reaction time 120 min)

$[Zn(II)]_0$/M	$[TAA]_0$/M	temp/°C	crystallite size/nm
0.1	0.1	50	3.8
0.1	0.1	70	4.0
0.1	0.1	90	4.1
0.4	0.1	70	3.5
0.1	0.4	70	4.2

ZnS particles of about 100 nm in size which uniformly cover the substrate. There was no significant change in morphology when the reaction time was extended to 240 min.

Structural Properties. Figure 9 shows XRD patterns of the deposited film and the precipitate after the reaction for 240 min. The thickness of the film is about 140 nm. Aside from the diffraction peaks from the ITO substrate, both the film and the precipitate show broad peaks which can be assigned to cubic ZnS,[48] since there are no characteristic peaks from hexagonal structure.[49] EDX analysis of the products revealed that the composition of both the film and the precipitate is close to stoichiometry. The average size of the crystallite has been estimated from the full-width at half-maximum of the (111) diffraction peak using Scherrer's equation. Those of the ZnS thin films deposited for 120 and 240 min were found to be about 4.0 nm, which is unchanged by the extension of the reaction time and similar to the value determined for the bulk precipitate under the same conditions. On the other hand, the film thickness increases with the reaction time. Therefore, it can be concluded that both the film and the precipitate have a nanocrystalline structure without appreciable crystal growth with reaction time. Table 1 summarizes the size of the crystallite measured for different deposition conditions. It is almost invariable by the reaction time, the temperature and the bath composition.

Figure 10 shows TEM images of ZnS precipitate and a ZnS thin film deposited on an ITO-coated glass. The precipitate formed after 120 min of reaction is made up of fine particles of ca. 4 nm in diameter, which is consistent with the result of XRD (Figure 10a). It should be noted that ZnS crystallites of the same size were found already after the reaction for only 5 min, indicating that these crystallites are almost instantaneously formed and do not grow further. Figure 10b shows a cross sectional view of a ZnS thin film. A dense and uniform ZnS layer is seen on the ITO layer. It can be seen from the close-up view in Figure 10b that the ZnS layer is made up with fine particles of the same size as those of the precipitate. The electron diffraction pattern of the ZnS layer (Figure 10c) shows diffuse rings as typically expected for nanocrystalline films. These rings

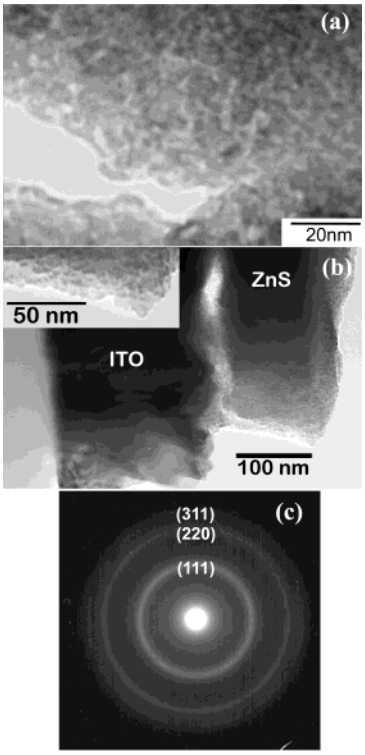

Figure 10. TEM images of ZnS precipitate formed in a 0.1 M $Zn(OAc)_2$ + 0.1 M TAA aqueous mixture after a reaction for 120 min (a), a cross section of a ZnS thin film deposited on an ITO-coated glass after a reaction for 300 min in the same reaction bath (b), and an electron diffraction (ED) pattern obtained for the ZnS thin film (c).

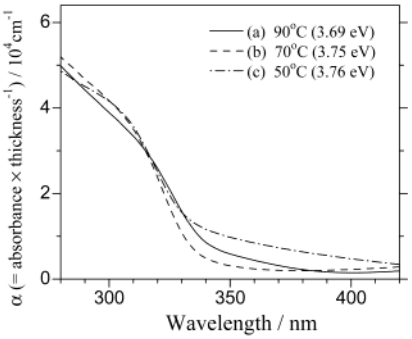

Figure 11. UV−vis absorption spectra of ZnS thin films deposited after the reaction for 120 min in 0.1 M $Zn(OAc)_2$ + 0.1 M TAA aqueous mixtures at 90 (a), 70 (b), and 50 °C (c). The spectra were normalized by dividing absorbance by the film thickness. The estimated band gap energies are given in parentheses.

can be assigned to β-ZnS. The same pattern has also been obtained for the ZnS precipitate.

Optical Properties. Figure 11 shows UV−vis absorption spectra of ZnS thin films deposited on glass substrates at 50, 70, and 90 °C after the reaction for 120 min. The thickness of the films were 39, 93 and 199 nm, respectively. These spectra were normalized by dividing absorbance by film thickness in order to express them in the apparent absorption coefficient (α). It is seen that these spectra almost coincide, indicating the constant density of the films grown at different temperatures. The absorption onsets of the films are well defined. The corresponding band gap energies (E_g) for direct transition of ZnS films were determined from the abscissa of the linear fittings to $(\alpha\, h\nu)^2$ vs $h\nu$ plots. Similar E_g values of 3.76, 3.75, and 3.69 eV were found for the films deposited at 50, 70, and 90 °C, respectively, being somewhat larger than the typical value

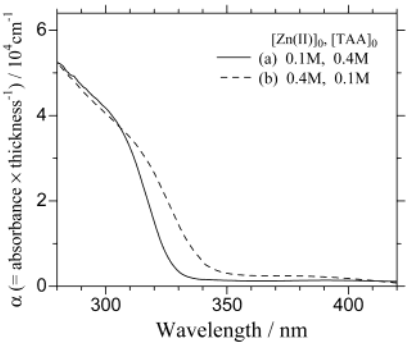

Figure 12. UV−vis absorption spectra of ZnS thin films deposited in the baths for which $[Zn(II)]_0$ and $[TAA]_0$ were adjusted to 0.4 and 0.1 M (a), and 0.1 and 0.4 M (b), respectively. The reactions were carried out at 70 °C and for 180 min. The spectra were normalized by dividing absorbance by the film thickness.

of the bulk ZnS (ca. 3.6 eV), due probably to the size quantization effect as expected from the nanocrystalline nature of the films. The small difference in E_g is in agreement with the lack of marked difference in the crystallite size with temperatures.

The absorption spectra of ZnS films prepared under the two extreme bath compositions, i.e., $[Zn(II)]_0/[TAA]_0 = 0.1$ M/0.4 M and 0.4 M/0.1 M, are also compared in Figure 12. The thicknesses of these films are 210 and 520 nm, respectively. The α values at the plateau are almost the same in the two spectra, although a certain red shift of absorption onset is noticed with the excess of [Zn(II)]. The unchanged α values for these films again indicate the constant density of the films.

Phenomenological Analysis

The kinetic analysis can be done first by considering the total concentrations of zinc and TAA in the overall deposition reaction (eq 3)

$$Zn(II) + CH_3CSNH_2 = ZnS + CH_3CN + 2\,H^+ \quad (3)$$

Assuming that the reverse reaction is negligible, the reaction rate can be then expressed by eq 4,

$$d[ZnS]/dt = k\,[Zn(II)]^n[TAA]^a \quad (4)$$

where n and a are the apparent reaction orders with respect to $Zn(OAc)_2$ and TAA concentrations, respectively. These concentrations are time dependent and decrease from the initial ones as the reaction proceeds. It appeared that the effect of the concentration to the rate of ZnS precipitation was symmetrical for zinc and TAA (Figure 2). This tells that the parameters n and a are close together. Equation 4 is thus transformed to

$$dP_t/dt = k[Zn(II)]^n[TAA]^n \quad (5)$$

where P_t is the concentration of zinc sulfide formed in the solution.

The relationship between reaction time and P_t can be derived by an iteration procedure as P_t can be calculated as the total sum of the progression sequence of ΔP_t (eq 6):

$$P_t = \sum_{s=1}^{s} \Delta P_t \cdot \Delta t = \sum_{s=1}^{s} k([Zn(II)]_0 - P_{s-1})^n([TAA]_0 - P_{s-1})^n \Delta t \quad (6)$$

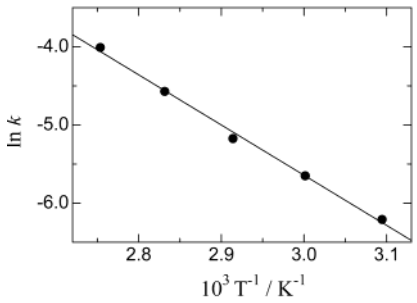

Figure 13. Arrhenius plot made from the relationship between the reaction temperature and rate constant k derived from eq 6. The activation energy of 53.4 kJ mol^{-1} was found for the precipitation reaction in the solution.

where $[Zn(II)]_0$ and $[TAA]_0$ are the initial concentrations of zinc salt and TAA, respectively, ΔP_t is the amount of precipitate formed in a short time Δt, and s is an integer and expressed by $s = t/\Delta t$. We find that an excellent fitting can be obtained for all precipitation curves as shown in Figure 2 with dotted lines by using the same set of parameters:

$$n = 0.637 \text{ and } k \text{ (at 70 °C)} = 5.66 \times 10^{-3}\,(\text{mol l}^{-1})^{1-2n}\,\text{min}^{-1}$$

The detailed procedure of the analyses described here is given in Appendix (i). Although we have examined the rate equation for the homogeneous precipitation of ZnS in acidic solutions proposed by Bowersox et al.,[50] this approach failed to analyze our data as shown in Appendix (ii).

Considering now the effect of temperature on the precipitation rate, good fitting is obtained by keeping the same value of the reaction order and changing just the value of the rate constant. The calculated curves by using the estimated k values (see Supporting Information Table 1S) are shown in Figure 1 as solid lines. Figure 13 shows the Arrhenius plot for the relationship between the rate constant and the reaction temperature. A good linear relationship is obtained. An activation energy of 53.4 kJ/mol has been determined from the slope of the Arrhenius plot for the ZnS precipitation in the present system, which is in the order typically expected for a chemical reaction.

Looking into the film deposition, we found in all cases that the thickness of the film follows the same dependence as that of the bulk precipitation process taking place in parallel and can be expressed simply as:

$$F_t = mP_t \quad (7)$$

where F_t is the film thickness at t and m is a proportionality factor [nm mM^{-1}]. Very nice fitting to the thickness data at all the temperatures are obtained by taking a unique m value of 3.17 nm mM^{-1} as indicated by the solid lines shown in Figure 3. It is important to note that the m value is temperature-independent within the present temperature range as long as the composition of the solution is kept as $[Zn(II)]_0/[TAA]_0 =$ 0.1 M/0.1 M.

Equation 7 successfully correlated the film growth and the precipitation by taking a single m value when the reaction temperature was varied. However, it is no longer valid to describe the film growth when the solution composition is changed, as noticed from the clear differences of the rates of the film growth between Figures 4a and 4b. We have therefore allowed the constant m to vary in eq 7 for these sets of data. Quite nice fitting to the experimental data points has been achieved for the curves with the optimized m values as shown

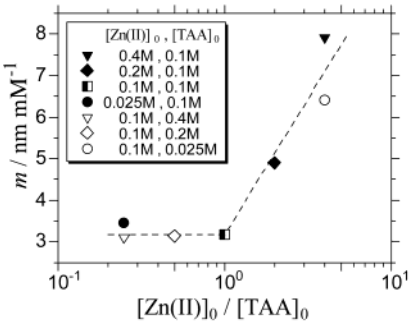

Figure 14. Relationship between the proportionality coefficient *m* derived from the curve fits in Figure 4 and the ratio of the initial concentrations of the two components in the reaction bath, $[Zn(II)]_0/[TAA]_0$, in a logarithmic scale.

in Figures 4a and 4b, indicating that the film growth is still proportional to the precipitation at a given bath composition. The *m* value has been found to vary with the bath composition. Those determined for the series in Figures 2, 4a and 4b are plotted versus the ratio of the initial concentrations of the two components, $[Zn(II)]_0/[TAA]_0$ in a logarithmic scale in Figure 14. When this ratio is lower than or equal to one, the value is fairly constant. However, when $[Zn(II)]_0/[TAA]_0$ becomes larger than one, namely, in the presence of an excess of Zn(II), the *m* value increases linearly.

Discussion

We have compared the rates of ZnS film growth and formation of precipitate in aqueous solutions containing $Zn(OAc)_2$ and TAA. Structural characterization revealed that both the film and the precipitate were made up of ZnS nanocrystallites with a diameter of ca. 4 nm, indicating that these nanocrystallites are common building units in both processes. These building units agglomerate in larger entities which can appear as the larger structures both in the precipitate and in the film. This aggregation process can lead to the formation of almost perfect spheres in the solution, which has been widely documented in the literature about the precipitation of ZnS using thioacetamide.[35−45] The internal structure of the spheres, which can be in some cases almost monodisperse, has been the matter of intensive debate, but their nanocrystalline nature has become a well-established knowledge by now.[40−43] Recently, Eshuis et al. has proposed a model considering four stages during the homogeneous precipitation of ZnS from zinc sulfate and TAA in acidic solution (Figure 15a).[43] According to this model, stage (i) corresponds to the formation of small particles with the diameter from 20 to 80 nm which are positively charged, stage (ii) to the aggregation of these particle to form string-shape units which consist of up to 20 particles, stage (iii) to the aggregation of these units to form perfect spheres as observed under the microscope, and stage (iv) to the formation of agglomerates of these spheres after a prolonged reaction time. The authors have claimed that the occurrence and the characteristics of these stages are strongly dependent on the experimental conditions. Comparison of our results concerning the homogeneous precipitation to their model has been made. The precipitate in the present study is made of ZnS nanocrystallites so that any structures formed at the higher stages are made of these elementary building units. Our results are also consistent with the other previous reports in which the ZnS particles in μm range are made of nanocrystallites in a diameter of a few tens of nanometers.[36,41] The difference is that the size of the building units is much smaller in our study (4 nm) compared to that in the model proposed by Eshuis et al. (20−80 nm).[43] In addition, we did not observe the string-shape units which are considered in the stage (ii) of the model. These differences may be due to the difference in the solution composition, which is mainly associated with the higher pH (4.5−6.5 instead of 1−2), and with the effect of anion (acetate instead of sulfate). For instance, it is known that the induction time for the formation of nuclei and the structure of resultant precipitate are affected by anion used in the system.[40,43]

One can note that $[Zn(II)]_0$, $[TAA]_0$, and the reaction temperature have little effect on the size of the building units in our case. However, the change in the morphologies of ZnS precipitate associated with the excess or dearth of Zn(II) in the bath clearly reflect the difference in the rate of aggregation of ZnS nanocrystallites, which is not explained by the model of Eshuis et al. The increase in the rate of aggregation with excess $[Zn(II)]_0$ can be explained by the difference of surface charge of ZnS nanocrystallites. Since the isoelectric point for spherical ZnS colloids has been reported either as pH 2.3[44] or 3,[38] ZnS particles should be negatively charged in our experimental condition (pH = 5∼6). However, it has also been found that the isoelectric point of ZnS colloid is affected not only by pH but also coexisting ions such as Zn^{2+} and $Zn(OH)^+$.[44] This means that the presence of these cations is expected to shift the surface charge positively because of their adsorption on the ZnS surface. Such an effect has also been observed for CdS colloids in solutions with a fixed pH where the isoelectric point shifts toward the higher pH upon increasing the concentration of coexisting cadmium ion.[44,51] One should note that these electrokinetic studies on the colloidal particles were performed separately from the synthesis of these colloids. In addition, it is known to take several hours to establish the equilibration of the surface charge.[44] At the present state of research, we are not sure how the exact surface potential of ZnS nanocrystallites can be determined in the systems where the homogeneous precipitation is continuously taking place. The detailed analysis of the surface charge of ZnS nanocrystallites is beyond the scope of the present study and is not to be discussed further. However, considering our experimental findings and previous studies on the surface potentials described above, it is most likely that the enhanced aggregation observed in the presence of excess zinc ion is attributed to the decreased repulsive electrostatic force between ZnS nanocrystallites owing to the surface charge neutralization.

Considering now the film formation, the building units are the same as those of the precipitate and the structure of the agglomerated grains appears to follow that of the precipitate in the solution. Films with larger structures are grown when larger particles are formed in the solution, indicating that the film growth also proceeds by the aggregation of the elementary units formed in the solution. This process is expressed as a cluster-by-cluster growth, which has been often claimed for the CBD of ZnS.[2,11,12] A contrasting behavior has been observed for the deposition of CdS, for which heterogeneous reactions at the surface lead to an atom-by-atom growth.[9,23,26] In this case, the film growth is accompanied by the growth of crystallites. Thus, the resultant films often are made of larger grains than those of the precipitate.

To complete the description of the film growth of ZnS, the significance of the coefficient *m* in eq 7 has to be considered. For ZnS nanocrystallites, the surface of the substrate can be regarded as that of a grain with an infinite radius. This assumption gives a basis to discuss the relationship between the growth of the film and the bulk reaction. At first thought,

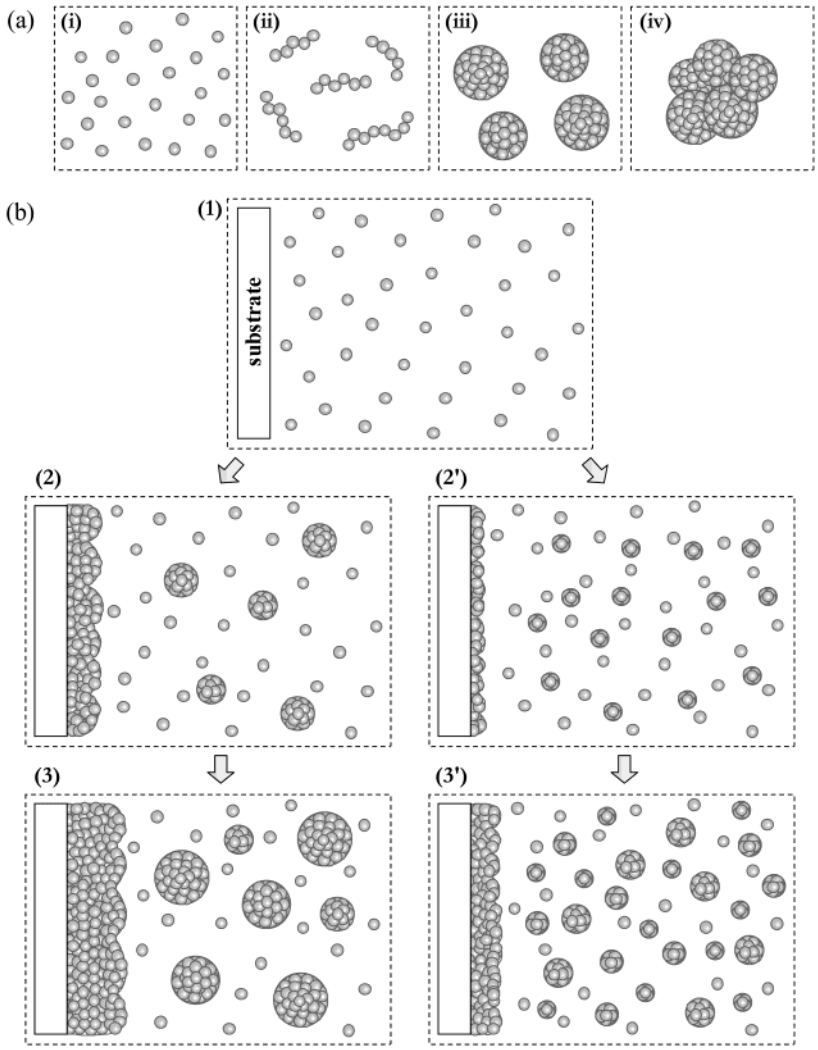

Figure 15. Schematic illustrations to describe the formation of colloidal ZnS particles according to the model proposed by Eshuis et al.[43] in which four stages are considered (a) and that summarizes both ZnS precipitation in the solution and a cluster-by-cluster growth of ZnS thin films in the present system (b). When the bath contains an excess of Zn(II), the rate of aggregation increases (high *m*), resulting in the formation of large ZnS particles as well as the high growth rate of ZnS thin films (pathway on the left-hand side). In the excess of TAA, the rate of aggregation decreases (low *m*), resulting in the formation of small ZnS particles and the slow growth of the film (pathway on the right-hand side). (See Discussion section of the text for detail.)

the thickness of the film appeared to be simply proportional to the mass of ZnS formed in the bulk of the solution. Thus, one might think that the difference in the film thickness of the two films prepared under the two extreme conditions (Figure 7), i.e., $[Zn(II)]_0/[TAA]_0 = 0.4$ M/0.1 and 0.1 M/0.4 M, was due to the difference in the density of the films, as neither the diameter nor the number of the particles formed in solution was variable for the global precipitated mass. However, it was clear that the apparent densities of these films were almost the same for the two films as the same apparent absorption coefficients were found from the absorption spectra (Figure 12). Obviously, a film of the same quality grew faster with the excess of $[Zn(II)]_0$ than the other case. In other words, the higher proportion of ZnS formed in the bath was fixed on the substrate as a film. It is necessary to look back to our experimental results to understand the mechanism for variation of *m*. When ZnS was precipitated under excess Zn(II), large spherical particles were formed (Figure 6). This result clearly indicates that the aggregation of nanocrystallites gets faster with an excess of Zn(II). Since the mass of the precipitate formed under the two extreme conditions is the same, the number of the particles should be less, while the average particle size should be larger in the bath containing excess Zn(II) than those of the other conditions. This idea is consistent with the morphology of the precipitate shown in Figure 6. Considering that the surface of the substrate acts in the same way as that of the particles formed in the solution, the attachment of ZnS nanocrystallites should take place not only to the ZnS particles formed in the bath but also to the substrate or the surface of the film. The increased rate of the aggregation therefore ends up with the formation of large particles in the bath as well as thick films on the substrate. While the rate of aggregation does not influence the total mass of the precipitate, it does influence the rate of the film growth as seen by the variation of *m*. Consequently, the coefficient *m* is most reasonably understood as a factor which reflects the rate of the aggregation of ZnS nanocrystallites on the substrate. In other words, the rate of the film growth is controlled by the probability for the nanocrystallites to stick to the substrate. The limitation to the rate of the film growth by the diffusion of ZnS nanocrystallites should also be ruled out since the activation energy found in the present study (53.4 kJ/mol) is typical for chemical reactions, as the diffusion-limited process should reveal a much smaller activation energy.[13,52]

Based on the results and discussion described above, the plausible mechanism for the homogeneous precipitation as well as the film growth of ZnS conditions in this work is depicted

in Figure 15b, comparing the two conditions with the same rate of the homogeneous precipitation, e.g., $[Zn(II)]_0/[TAA]_0 = 0.4$ M/0.1 and 0.1 M/0.4 M. Each step indicates (1) formation of primary building units by the continuous chemical formation of ZnS in the bath, (2) film growth by the accumulation of the building units paralleled with the formation of the spherical particles (aggregates), (3) progression of the same processes as (2). In steps (2) and (3), the pathway on the left-hand side is the case with the high aggregation rate and that on the right is with the low rate. Note that step (1) continues to take place also in steps (2) and (3), and it should last as long as the bath is supersaturated. The particles made as agglomerates of the ZnS nanocrystallites grow by capturing the primary building units that are formed around them. At the same time, the same building units diffuse and stick to the surface of the substrate to grow a film of ZnS. Consequently, when the bath contains an excess of Zn(II), the rate of aggregation increases, resulting in the formation of large ZnS particles as well as a high growth rate of ZnS thin films. The high m value found for this situation reflects the high proportion of ZnS formed into a film, namely, the high efficiency of the film growth. On the other hand, the rate of aggregation becomes low in the excess of TAA, resulting in the formation of smaller ZnS particles and the low rate of the film growth (= low efficiency of the film growth).

To go further in the discussion of the reaction mechanism, it is interesting to consider more precisely the phenomenological law describing the precipitation kinetics. What could be the meaning of the symmetry between total zinc concentration and thioacetamide? Looking back to the literature about zinc sulfide precipitation using TAA, two reaction mechanisms have long been proposed depending on the pH of the solution.[43] At a low pH (<2.5), the reaction is considered to be controlled by the rate of hydrolysis of TAA molecules leading to the formation of hydrogen sulfide molecules. Then zinc ions react with hydrogen sulfide to form ZnS. As a consequence, this reaction is an indirect reaction between zinc ions and TAA. Its rate is also affected by the pH of the solution, with an increase when the pH decreases. At the higher pH (>2.5), the process is considered to follow a direct reaction path,[50] from which Peeters et al. claimed that the reaction is controlled by the formation and decomposition of Zn^{2+}−TAA complexes.[46] As the pH of the solution in the present study is higher than 2.5, the latter route via the complex formation should better be considered.

Complex formation can be written as resulting from general chemical equilibria:

$$Zn^{2+} + n\mathrm{TAA} \rightleftarrows Zn(TAA)_n^{2+} \qquad (8)$$

If we consider that the rate-limiting step for ZnS formation is the decomposition of the complex and that the complexation equilibrium is realized, one can write that

$$P_t = k[Zn(TAA)_n^{2+}] = k[Zn^{2+}][TAA]^n/\beta \qquad (9)$$

where β is the overall complexation coefficient of zinc with TAA, expressed by $\beta = [Zn(TAA)_n^{2+}]/[Zn^{2+}][TAA]^n$. The observation of a symmetrical effect between $[Zn(II)]_0$ and $[TAA]_0$ on the precipitation process indicates that n should be one. As a consequence, a complete symmetry is simply obtained by considering the formation of a 1:1 complex species between Zn^{2+} and TAA. This complex may involve one acetate ligand, since the formation of monoacetato complexes of Zn^{2+} is favored under the pH range of our experiments.[53] In the previous report on the reaction between metal ions (Pb^{2+}, Cd^{2+}, Co^{2+}) and TAA in acetate buffered solutions, decomposition of 1:1 metal−thioacetamide complexes was also suggested as the rate-determining step.[46]

This analysis shows that the rate-limiting step may be related to the formation of "individual" molecules of ZnS which then gather to form ZnS nuclei. The individual nature of the reacting species explains the single crystalline nature of the ZnS nanocrystalline building blocks with invariable size. This hypothesis of nucleation controlled growth in the case of ZnS precipitation is in good agreement with the conclusions of recent mechanistic studies.[43] In the classical approach, the "individual" molecules and the building blocks were not distinguished. In a mechanism to yield monodispersed colloidal particles, further seed formation is avoided after initial seeds are made. In this case, once a critical supersaturation state is attained, the degree of supersaturation relaxes to prevent further nucleation. Newly generated "individual" molecules or building blocks are consumed only for the growth of the initially created seed particles, via a heterogeneous process.[54] In the present study, we have chosen a system in which formation of ZnS nanocrystallites continues to take place by maintaining the degree of supersaturation at a sufficiently high level. These ZnS nanocrystallites are actually the only building units of the film and precipitate, which are consumed not only for the growth of the existing agglomerates but also by formation of new agglomerates, as seen from the polydisperse nature in the size of the ZnS colloidal particles.

Conclusion

In this work we have established general laws for the precipitation of ZnS in aqueous mixture of zinc acetate and thioacetamide aqueous solutions and succeeded for the first time in establishing a correlation with the growth of films by the so-called chemical bath deposition method. With the help of structural characterizations, it has been clarified that the building units both for the film and the precipitate are nanocrystallites formed in the solution. The film growth in the present system proceeds by the accumulation of nanocrystallites formed in the solution, namely, in a way called a cluster-by-cluster manner. In that sense one can consider this process as leading to nanostructured materials. The film growth is under the control of the homogeneous precipitation in the solution as found by the kinetic analyses both for the homogeneous precipitation and the film growth. The rate of the film growth is affected not only by the rate of the formation of ZnS nanocrystallites but also by that of the aggregation of nanocrystallites at the substrate. Further studies are needed to determine the factors that control the diameter of the elementary particles. One of the main contributions from the present work is the proposal of a phenomenological kinetic law, which has been explained by assuming that the rate-limiting step is the nucleation step from 1:1 complex species between Zn^{2+} and TAA, involving probably one acetate ligand. Contrary to the approach in the classical theories, nucleation is maintained in the course of the reaction. The aggregation process is another important factor that controls the film growth in the CBD processes in a cluster-by-cluster mechanism. The nature of the complex species involved in the nucleation step, the origin of size control in the initial crystallite formation, and the transitions between various stages of the aggregation processes are still open questions.

Acknowledgment. The present work is partly defrayed by the Industrial Technology Research Grant Program in '01 from New Energy and Industrial Technology Development Organization (NEDO) of Japan (01B64002c) and the Grant-in Aid for

Scientific Research (B) No. 13555236 from the Japan Society for the Promotion of Science. The authors thank Mr. Hiroshi Nakamura and Ms. Hiromi Iijima of Gifu University (Japan) for preparation of ZnS samples, and Prof. Takashi Sugiura of Gifu University for the fruitful discussion and technical assistance. K.Y. is grateful to Research Fellowships of the Japan Society for the Promotion of Science for Young Scientists. T.Y. is grateful to Centre National de la Recherche Scientifique (CNRS, France) for the financial support for a research stay at the ENSCP.

Appendices

(i) Kinetic Analysis of Homogeneous Precipitation in $Zn(OAc)_2$−TAA System. According to Peeters et al., in an aqueous mixture of metal cations and TAA in the pH range 5−6 at 80 °C, the reaction products identified are acetonitrile and metal sulfide.[46] Later, Sugimoto et al. also have reported that ^{1}H NMR and FT-IR analyses revealed the formation of acetonitrile as a byproduct during the synthesis of CdS colloids in a condensed suspension of $Cd(OH)_2$ containing TAA.[47] Thus, the overall reaction for the formation of ZnS is most likely expressed as eq A1.

$$Zn(OAc)_2 + CH_3CSNH_2 = ZnS + CH_3CN + 2HOAc \quad (A1)$$

The rate of ZnS formation as a function of time can be expressed as:

$$P_t = k[Zn(II)]^n[TAA]^a \quad (A2)$$

where n and a are the apparent reaction orders. However, we have found that the precipitation reaction can be phenomenologically well described using the following rate equation (same as eq 5 in the text):

$$\frac{dP_t}{dt} = k[Zn(II)]_t^n[TAA]_t^n \quad (A3)$$

Equation A3 can be rewritten as eq A4,

$$\frac{dP_t}{dt} = k([Zn(II)]_0 - P_t)^n([TAA]_0 - P_t)^n \quad (A4)$$

where $[Zn(II)]_0$ and $[TAA]_0$ are the initial concentrations of zinc salt and TAA, respectively. Therefore, the amount of ZnS precipitates ΔP_t formed in a short time Δt can be expressed by eq A5:

$$\Delta P_t = k([Zn(II)]_0 - P_t)^n([TAA]_0 - P_t)^n\Delta t \quad (A5)$$

Then, P_t can be calculated as the total sum of the progression sequence of ΔP_t (eq A6, same as eq 5 in the text)

$$P_t = \sum_{s=1}^{s} \Delta P_t\Delta t = \sum_{s=1}^{s} k([Zn(II)] - P_{s-1})^n([TAA]_0 - P_{s-1})^n\Delta t \quad (A6)$$

where s is an integer and expressed by $s = t/\Delta t$. As noted earlier, our first attempt was to apply a second-order rate equation ($n = a = 1$ in eq A2) to the experimental data. However, a unique rate constant k which satisfies all of the data with various $Zn(OAc)_2$ and TAA concentrations could not be found. Since the order of the reaction with respect to $[Zn(II)]_t$ and $[TAA]_t$ appeared to be the same, the analyses were made for each combination of $[Zn(OAc)_2]_0$ and $[TAA]_0$, i.e., one of the concentrations was 0.1 M and the others were varied as 0.4, 0.2, 0.1, and 0.025 M. Then, we have phenomenologically analyzed the experimental data by taking variable n and determined the values of n and k by least-squares method, i.e., $\sum (P_{t,ex} - P_{t,cal})^2$ to become minimum, where $P_{t,ex}$ and $P_{t,cal}$ refer to the amounts of ZnS precipitates which were experimentally found and the calculated values of P_t using eq A6, respectively. Such an analysis has led to $n = 0.637$ and k (at 70 °C) $= 5.66 \times 10^{-3}$ (mol/L)$^{1-2n}$ min^{-1} as the most suitable values for the data plots in Figure 2.

(ii) Calculation of P_t Based on the Previously Reported Rate Equation. According to the previous study of Bowersox et al. on the homogeneous precipitation of ZnS under weak acidic conditions (pH values between 4.5 and 6.3), the rate equation is given by eq A7,

$$-\frac{d[Zn(II)]}{dt} = k\frac{[Zn(II)][TAA]}{[H^+]^{1/2}} \quad (A7)$$

where k is the rate constant and equals to 4.2×10^{-4} L$^{1/2}$ mol$^{-1/2}$ min^{-1} at 90 °C.[50] Taking the activation energy of 19 kcal/mol (= 79.5 kJ/mol) reported in their paper, k at 70 °C is calculated to be 9.04×10^{-5} L$^{1/2}$ mol$^{-1/2}$ min^{-1}. We tried to compare our data of precipitation (Figure 2) to the theoretically calculated amount of precipitates from this rate equation at 70 °C for various combinations of $[Zn(II)]_0$ and $[TAA]_0$. Following a procedure similar to that described in Appendix (i), eq A7 is rewritten as eq A8:

$$P_t = \sum_{s=1}^{s} \Delta P_t\Delta t = \sum_{s=1}^{s} \frac{k([Zn(II)]_0 - P_{s-1})([TAA]_0 - P_{s-1})}{[H^+]^{1/2}}\Delta t \quad (A8)$$

The values of $[H^+]$ were taken from the relationship between pH and the reaction time for various bath compositions, which were measured separately (see Supporting Information, Figure 1S). The experimental data are compared to the calculated curves obtained by eq A8 for each combination of the concentrations of $[Zn(II)]_0$ and $[TAA]_0$ (see Supporting Information, Figure 2S). Although the experimental values are in a rather good agreement with the theoretically calculated curve only when $[Zn(II)]_0 = [TAA]_0 = 0.1$ M, all the values for other bath compositions are out of the theoretically calculated curves. This result clearly indicates that the precipitation reaction in the present system does not follow the rate equation proposed by Bowersox et al. (eq A7).

Supporting Information Available: Two figures for the change of pH with reaction time for different bath compositions, one figure which adds a fitting curve according to the rate equation previously reported by Bowersox et al., one table listing the reaction rate constants determined for the precipitation of ZnS in the phenomenological analysis (3 pages). This material is available free of charge via the Internet at http://pubs.acs.org.

References and Notes

(1) Yoshimura, M.; Suchanek, W. L.; Byrappa, K. *MRS Bull.* **2000**, *25*, 17.

(2) Lincot, D.; Froment, M.; Cachet, H. In *Advances in Electrochemical Science and Engineering*; Alkire, R. C., Kolb, D. M., Eds.; Wiley−VCH: New York 1999, Vol. 6, 165.

(3) Ristov, M.; Sinadinovski, G.; Mitreski, M.; Ristova, M. *Sol. Energy Mater. Sol. Cells* **2001**, *69*, 17.

(4) Grozdanov, I. *Appl. Surf. Sci.* **1995**, *84*, 325.

(5) Yoshida, T.; Yamaguchi, K.; Toyoda, H.; Akao, K.; Sugiura, T.; Minoura, H.; Nosaka, Y. *Electrochem. Soc. Proc.* **1997**, *97*−*20*, 37.
(6) Bayón, R.; Guillén, C.; Martínez, M. A.; Gutiéerez, M. T.; Herrero, J. *J. Electrochem. Soc.* **1998**, *145*, 2775.
(7) Bayón, R.; Hernández-Mayoral, M.; Herrero, J. *J. Electrochem. Soc.* **2002**, *149*, C59.
(8) Supothina, S.; De Guire, M. R. *Thin Solid Films* **2000**, *371*, 1.
(9) Ortega-Borges, R.; Lincot, D. *J. Electrochem. Soc.* **1993**, *140*, 3464.
(10) Gorer, S.; Hodes, G. *J. Phys. Chem.* **1994**, *98*, 5338.
(11) Froment, M.; Lincot, D. *Electrochim. Acta* **1995**, *40*, 1293.
(12) O'Brien, P.; McAleese, J. *J. Mater. Chem.* **1998**, *8*, 2309.
(13) Doña, J. M.; Herrero, J. *J. Electrochem. Soc.* **1994**, *141*, 205.
(14) Nakada, T.; Mizutani, M. *Jpn. J. Appl. Phys.* **2002**, *41*, L165.
(15) Nakada, T.; Mizutani, M.; Hagiwara, Y.; Kunioka, A. *Sol. Energy Mater. Sol. Cells* **2001**, *67*, 255.
(16) Nair, P. K.; Nair, M. T. S. *Semicond. Sci. Technol*. **1992**, *7*, 239.
(17) Mokili, B.; Charreire, Y.; Cortes, R.; Lincot, D. *Thin Solid Films* **1996**, *288*, 21.
(18) Nicolau, Y. F.; Dupuy, M.; Brunel, M. *J. Electrochem. Soc.* **1990**, *137*, 2915.
(19) Kanniainen, T.; Lindroos, S.; Prohaska, T.; Friedbacher, G.; Leskelä, M.; Grasserbauer, M.; Niinistö, L. *J. Mater. Chem.* **1995**, *5*, 985.
(20) Ortega-Borges, R.; Lincot, D.; Vedel, J. In *Proceedings of the 11th EC Photovoltaic Solar Energy Conference*, 1992, p 862.
(21) Oladeji, I. O.; Chow, L. *Thin Solid Films* **1999**, *339*, 148.
(22) O'Brien, P.; Otway, D. J.; Smyth-Boyle, D. *Thin Solid Films* **2000**, *361*−*362*, 17.
(23) Yamaguchi, K.; Yoshida, T.; Sugiura, T.; Minoura, H. *J. Mater. Res.* **1998**, *13*, 917.
(24) Xu, D.; Xu, Y.; Chen, D.; Guo, G.; Gui, L.; Tang, Y. *Adv. Mater.* **2000**, *12*, 520.
(25) Penner, R. M. In *Electrochemistry of Nanomaterials*; Hodes, G., Ed.; Wiley−VCH, Weinheim, 2001; Chapter 1, p 1.
(26) Yamaguchi, K.; Yoshida, T.; Sugiura, T.; Minoura, H. *J. Phys. Chem. B* **1998**, *102*, 9677.
(27) Hodes, G. In *Physical Electrochemistry: Principles, Methods, and Applications*; Rubinstein, I., Ed.; Marcel Dekker: New York, 1995; Chapter 12, p 515.
(28) Yoshida, T.; Minoura, H. *Adv. Mater.* **2000**, *16*, 1219.
(29) De Tacconi, N. R.; Boyles, C. A.; Rajeshwar, K. *Langmuir* **2000**, *16*, 5665.
(30) Stickney, J. L. *Electroanal. Chem.* **1999**, *21*, 75.
(31) Das, S. K.; Morris, G. C. *Sol. Energy Mater. Sol. Cells* **1993**, *28*, 305.
(32) Kampmann, A.; Cowache, P.; Lincot, D.; Vedel, J. *J. Electrochem. Soc.* **1999**, *146*, 150.
(33) Murase, K.; Uchida, H.; Hirato, T.; Awakura, Y. *J. Electrochem. Soc.* **1999**, *146*, 531.
(34) Lovergine, N.; Prete, P.; Leo, G.; Calcagnile, L.; Cingolani, R.; Mancini, A. M.; Romanato, F.; Drigo, A. V. *Cryst. Res. Technol.* **1998**, *33*, 183.
(35) Bredol, M.; Merikhi, J. *J. Mater. Sci.* **1998**, *33*, 471.
(36) Vacassy, R.; Scholz, S. M.; Dutta, J.; Plummer, C. J. G.; Houriet, R.; Hofmann, H. *J. Am. Ceram. Soc.* **1998**, *81*, 2699.
(37) Chiu, G. *J. Colloid Interface Sci.* **1981**, *83*, 309.
(38) Wilhelmy, D. M.; Matijevic, E. *J. Chem. Soc., Faraday Trans. 1* **1984**, *80*, 563.
(39) Williams, R.; Yocom, P. N.; Stofko, F. S. *J. Colloid Interface Sci*. **1985**, *106*, 388.
(40) Celikkaya, A.; Akinc, M. *J. Am. Ceram. Soc*. **1990**, *73*, 245.
(41) Celikkaya, A.; Akinc, M. *J. Am. Ceram. Soc* **1990**, *73*, 2360.
(42) Sugimoto, T.; Dirige, G. E.; Muramatsu, A. *J. Colloid Interface Sci.* **1996**, *180*, 305.
(43) Eshuis, A.; van Elderen, G. R. A.; Koning, C. A. *Colloids Surf. A: Physicochem. Eng. Aspects* **1999**, *151*, 505.
(44) Nicolau, Y. F.; Menard, J. C. *J. Colloid Interface Sci.* **1992**, *148*, 551.
(45) T. Nomura, Y. Kousaka, M. Alonso and M. Fukunaga, *J. Colloid Interface Sci.* **2000**, *223*, 179.
(46) Peeters, O. M.; Blaton N. M.; De Ranter, C. J. *J. Chem. Soc., Perkin Trans. 2* **1978**, 23.
(47) Sugimoto, T.; Dirige, G. E.; Muramatsu, A. *J. Colloid Interface Sci.* **1995**, *176*, 442.
(48) Joint Committee on Powder Diffraction Standards, Card 5−566.
(49) Joint Committee on Powder Diffraction Standards, Card 5−492.
(50) Bowersox, D. F.; Smith, D. M.; Swift, E. H. *Talanta* **1960**, *3*, 282.
(51) Guindo, M. C.; Zurita, L.; Durán, J. D. G.; Delgado, A. V. *Mater. Chem. Phys.* **1996**, *44*, 51.
(52) Lincot, D.; Vedel, J. *Proceedings of 10th EC Photovoltaic Solar Energy Conference* **1991**, 931.
(53) Dean, J. A. *Lange's Handbook of Chemistry*, 14th ed.; McGraw-Hill: New York, 1992; Section 8.
(54) Lamer, V. R.; Dinegar, R. H. *J. Am. Chem. Soc.* **1950**, *72*, 4847.